JOURNAL OF PROPULSION AND POWER
Vol. 24, No. 2, March–April 2008

Preliminary Study of Shock Train in a Curved Variable-Section Diffuser

Hui-jun Tan* and Shu Sun†
Nanjing University of Aeronautics and Astronautics, 210016 Nanjing, People's Republic of China

DOI: 10.2514/1.31981

Wind-tunnel tests are conducted to study the characteristics of the shock train in the curved variable-section diffuser for hypersonic inlets. The test model is equipped with a forebody, a contracting entrance, a dump mixing duct, and an aft plug. Tests are performed at nominal freestream Mach numbers of 4.0, 5.0, and 6.0, and the corresponding inlet Mach numbers of the diffuser are 2.05, 2.59, and 3.06, respectively. Results indicate that at an inlet Mach number of 2.05, the surface pressure distributions in the shock train are similar at different backpressure ratios and can be well predicted by the modified Waltrup formula, but the length of the shock train is increased by 32% due to the curved duct, the incident shock waves, and the incident expansion waves at the inlet plane. At higher inlet Mach numbers, the similarity disappears and the distributions of the surface pressure are not easy to predict. At different measurement points in the shock train, the instantaneous surface pressures vary obviously and almost synchronously, suggesting the oscillatory motions of the shock train. At an inlet Mach number of 2.59, the base frequency of the oscillations is about 19 Hz and the maximum fluctuating range of the instantaneous surface pressure is as high as 21.6% of the ideal pressure rise of the shock train. The static pressure fluctuations at different points in the shock train correlate strongly but are almost unrelated with those of the exit survey point, which indicates that the oscillation of the shock train is not likely induced by the pressure fluctuations far downstream of the shock train.

Nomenclature

C_{mb}	=	coefficient introduced to the Waltrup formula
D	=	diameter or equivalent diameter of the duct
H	=	height of the rectangular duct
Ma	=	Mach number
p	=	static pressure
p_{pt}	=	pitot pressure
p_t	=	total pressure
Re	=	Reynolds number
s	=	arc length of the central line from the inlet section of the diffuser
θ	=	boundary-layer momentum thickness
σ	=	total pressure recovery coefficient

Subscripts

e	=	exit station of the diffuser
0	=	freestream station
2	=	inlet station of the diffuser

Introduction

THE shock train in ducts is a complex phenomenon that is frequently encountered in a supersonic pressure-gain process. It is characterized by strong shock/boundary-layer interactions and a finite adverse pressure gradient in a finite flow region [1]. The shock train appears in a variety of fluid devices such as supersonic inlets [2–4], isolators of scramjets [5,6], and diffusers of supersonic wind tunnels [7], to name a few. On many occasions, the streamwise size and the aerodynamic performance of fluid devices are determined to a great extent by the nominal length, static pressure recovery, and total pressure recovery of the shock train. Consequently, this specific phenomenon has received increasing attention. In recent years, much has been learned of the flow patterns and the static pressure distributions of the shock train from both experimental and numerical research [8–18]. However, these investigations have been conducted mainly on the shock train in straight ducts. Little has been done on the shock train in curved ducts, except the preliminary numerical analysis on two-dimensional curved ducts with a constant cross-sectional area [19]. Actually, numerical and experimental studies of supersonic inlets or hypersonic inlets with curved ducts were reported since the 1970s, such as the P8 inlet developed by NASA [20], multiscoop inlet of a dual-combustor ramjet (DCR) [21], translating-central-body inlet of GTX [22], two-dimensional inlet of HYPR [23], variable geometry axisymmetric inlet of ATREX [24], etc. But the researchers just used curved diffusers passively to meet the general arrangement constraints of the propulsion system. Their studies focused on performance characterizations and performance enhancements of the inlets. No particular interests were shown in the shock train in curved ducts (Fig. 1). The flow pattern, the streamwise length, the static pressure recovery, and the total pressure recovery characteristics of the shock train in curved ducts are still left unknown. When a curved diffuser is used, what benefits will the inlets gain or what disbenefits will the inlets have to bear? There was no affirmative answer till now. In addition, little work has addressed the self-excited oscillations of the shock train. Present knowledge of the unsteady behaviors of the shock train is rather limited and many physical aspects, including the oscillating mechanism, are not well understood. Reference [25] investigates the oscillatory characteristics of the shock train in a rectangular straight duct, but the inlet Mach number lies below 1.75 and is not a typical value for isolators of hypersonic inlets. Because of the periodical changes of instantaneous static pressure, Mach number, and static temperature accompanied by the shock-train oscillations, the operating stability of the engine is possibly threatened and the structural strength is likely weakened. Therefore, a more thorough investigation is highly needed in this research field.

The current paper describes the experimental testing of a curved variable-section diffuser at inlet Mach numbers of 2.08, 2.59, and 3.06. The time-averaged and instantaneous distributions of surface static pressure and exit pitot pressure are analyzed. The objectives of the test program reported herein are to establish a preliminary knowledge of the behavior of the shock train in curved ducts and to provide a basic comparison with the shock train in straight ducts.

Received 6 May 2007; revision received 15 July 2007; accepted for publication 11 September 2007. Copyright © 2007 by Hui-jun Tan. Published by the American Institute of Aeronautics and Astronautics, Inc., with permission. Copies of this paper may be made for personal or internal use, on condition that the copier pay the $10.00 per-copy fee to the Copyright Clearance Center, Inc., 222 Rosewood Drive, Danvers, MA 01923; include the code 0748-4658/08 $10.00 in correspondence with the CCC.

*Associate Professor, College of Energy and Power Engineering.
†Postdoctoral Fellow, College of Energy and Power Engineering.

a) Curved duct in supersonic inlets

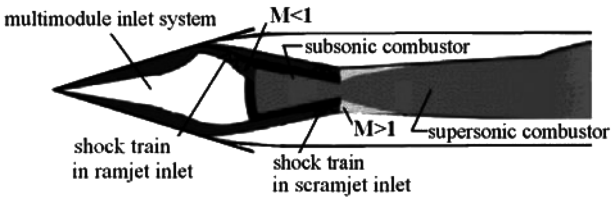

b) Curved ducts in the multimodule inlet system for a dual-combustor ramjet

Fig. 1 Shock train in curved ducts.

Experimental Setup

Wind Tunnel and Test Conditions

The experiments were conducted in a pulse-type combustion-heated wind tunnel. Gaseous fuel ($H_2 + N_2$) and oxidizer ($O_2 + N_2$) are stored in a pair of Ludwieg tubes. At the end of each tube is a quick-acting valve. The gases are discharged into an uncooled combustion heater in which combustion takes place and the desired enthalpy and pressure can be obtained. The mole fraction of oxygen after combustion heating remains at 0.21, just the same as in the atmosphere.

The test chamber is fully closed with schlieren glass windows for optical access. An axisymmetric converging–diverging supersonic nozzle with a diameter of 600 mm at the exit is located upstream of the test chamber, which provides different nominal freestream Mach numbers of 4.0, 5.0, and 6.0 with interchangeable throats. According to wind-tunnel calibrations, the diameter of the uniform flow region at the exit of the nozzle is about Φ440 mm and greater than Φ320 mm at the station that is 500 mm downstream, and the usable run time is greater than 200 ms. Freestream parameters at different test points are listed in Table 1.

Experimental Model

The test model used in the experiments simulates the inlet system for the ramjet module of a dual-combustor ramjet. The inlet is designed for a shock-on-lip Mach number of 6.0 and for a self-starting Mach number of 3.0. The inlet consists of an external compression cone, an internal contracting duct, and a diverging diffuser. The external compressions are accomplished by a cone surface with two turnings, of which the initial half-angle is 14 deg and the two following turning angles are both 5 deg. The total area contraction ratio of the inlet is 7.0 and the internal one is 1.5. Downstream of the throat of the inlet, a curved variable-section duct with an area ratio (exit area to inlet area) of 1.4 is located and serves as the diffuser (Fig. 2). The cross-sectional shape of the diffuser transits smoothly from a partial annular with a central angle of 25 deg at the inlet station to a breadlike shape at the exit station. The arc length of the diffuser central line is $7.8D$ and the vertical offset of the inlet section to the exit section is $3.0D$, where D denotes the average hydraulic diameter of the duct. The minimum curvature radius of the duct central line is $2.5D$ and the corresponding station is $1.3D$ downstream of the inlet section. The efflux angle of the duct is 30 deg.

Table 1 Wind-tunnel test conditions

Property	Test point 1	Test point 2	Test point 3
Nominal Mach number	4	5	6
Total pressure (10^6 Pa)	1.5	2.5	3.0
Total temperature, K	900	1360	1650
Specific heat ratio	1.37	1.36	1.35
Unit Reynolds number	9.57×10^6/m	6.59×10^6/m	3.65×10^6/m

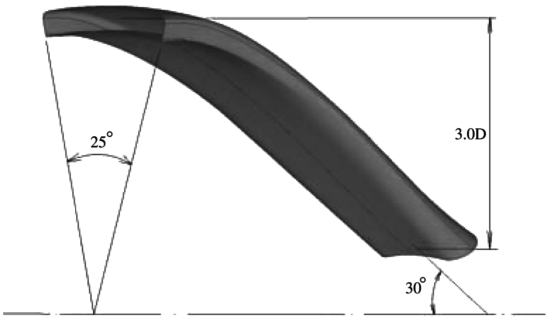

Fig. 2 Curved variable-section diffuser.

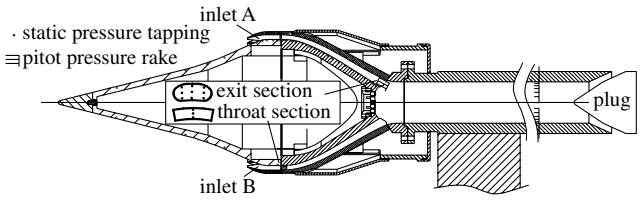

Fig. 3 Wind-tunnel test model.

Figure 3 illustrates the test model in which the full flowpath of two inlets for the ramjet is embodied. The cowl-lip diameter of the model is 300 mm. Two streams captured by the inlets impinge at the dump combustor and are discharged through a long straight duct for which the slenderness ratio is 10:1. A conical plug is placed at the end of the straight duct. The backpressure of the inlet thus can be varied by changing the position of the plug. The position of the conical plug is identified by the throttling ratio (TR), defined as the ratio of the throat area near the plug to the cross-sectional area of the straight duct. During tests, the throttling ratio can be varied between 0% (fully opened) and 100% (fully closed). What's more, each experiment is repeated twice for credible results.

Experimental Measurements

Instantaneous static pressure measurements are performed by 48 dynamic pressure (Kulite®) transducers: 27 stations on the central-body-side surface and 21 stations on the cowl-side surface of inlet A, to obtain the flow pattern inside the curved diffuser. To minimize the influence of installation flushness of pressure transducers, step holes are drilled perpendicularly to the model surface. The small end of the step hole is flush with the model surface without any protrusion and the larger end is connected with the transducer. Pitot pressure rakes are installed at the end of the throat of inlet B and at the exit of inlet A to obtain time-accurate local total pressures and local Mach numbers. Also, several dynamic pressure gauges are used to monitor the operating process of the wind tunnel, such as the action of hydrogen value, the action of oxygen value, and the establishment of total pressure in the prechamber.

The data sampling frequency is 11 kHz. To obtain the concerned instantaneous pressure information and to also ensure that the entire operating process of the wind tunnel is monitored, the sampling process lasts for 3 s. As far as the pressure gauges are concerned, the cutoff frequency is as high as 50 kHz. But during tests, the chamber in the sensor and the conduit degrade the frequency response of the data acquisition system. The volume of the chamber in the sensor is less than 40 mm^3 and the longest conduit used does not exceed 100 mm. The cutoff frequency f_0 can be calculated by the following formula:

$$f_0 = a\sqrt{\frac{r^2}{4\pi l(V + 4r^2 l/\pi)}}$$

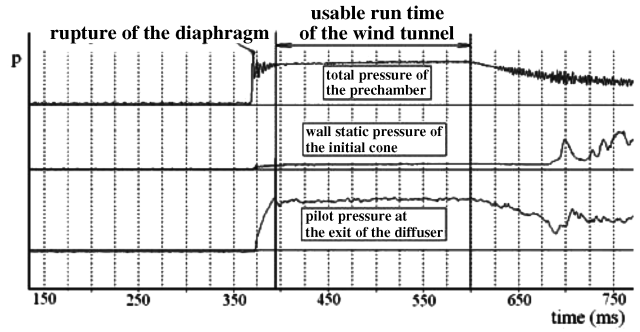

Fig. 4 Typical time sequence of the experiments.

where a is the local sound speed, l is the length of the conduit, r is the inner diameter of the conduit, and V is the volume of the chamber in the sensor. When calculating f_0, the largest values of l and V and a relative small value of a (300 m/s) are used so that a conservative cutoff frequency is obtained as 1159 Hz. In general, the cutoff frequency of the data acquisition system should be three times the interested frequency of the signal or higher. Therefore, in this paper, the analysis of a dynamic signal less than 386 Hz is authentic. Figure 4 shows a typical time sequence of the experiments, in which zero on the time axis represents the start of the data sampling process. More details about the test model and the experimental setup can be found in [26].

Results and Discussion

Distributions of Time-Averaged Surface Pressure

The time-averaged surface pressure is obtained from the time history data with an integration period of 150 ms. Because of the curvature of the duct, in the following discussion, a streamwise coordinate that is normalized in the style shown in Fig. 5 is used, where $s/D = 0$ denotes the inlet section and $s/D = 7.8$ denotes the exit section of the diffuser.

Figure 6 shows the normalized static pressure distributions along the cowl-side surface and the central-body-side surface of the diffuser at different throttling ratios. The freestream Mach number is 4.0. The curves are numbered in a throttling-ratio ascending style and curves 0–6 correspond to TR = 0.0, 76.7, 79.7, 81.8, 83.1, 84.3, and 84.7%, respectively. The shock train is not formed in the diffuser at TR = 0.0%, due to the free-pressure boundary condition at the exit. When TR increases to 76.7%, the shock train appears at the rear of the diffuser and continues to shift upstream with the augment of TR. It can be observed from curves 1–3 that the time-averaged surface pressures on both sides climb up smoothly along the flow direction and almost overlap with each other. Things begin to change when the shock train originates from the forepart of the duct, in which the surface curvature is larger (curves 4–6). Static pressure distributions of the central-body-side surface still take on a smooth and stable trend, but the pressure distributions of the cowl-side surface fluctuate remarkably, which suggests the change of flow pattern of the shock train [19]. But at the region of $s/D > 6.0$ of curves 4–6, the static pressure distributions on two side surfaces almost coincide with each other. The aforementioned characteristics of the surface pressure distributions can be interpreted as follows through relating them to the flow pattern of the shock train (Fig. 7):

1) When located at the rear of the diffuser, the shock train is symmetric to some extent, as a result of little local surface curvature and a low upstream Mach number (about 2.08). The fore legs near both the cowl-side surface and the central-body-side surface of each bifurcated shock are positioned closely in the streamwise direction. The supersonic core flow is contained in the duct without apparent deflection and there exist thick boundary layers near both sides. Therefore, the violent pressure fluctuations of the core flow can be well buffered before impressing on the walls, which results in the smoothly and symmetrically distributed time-averaged surface pressures.

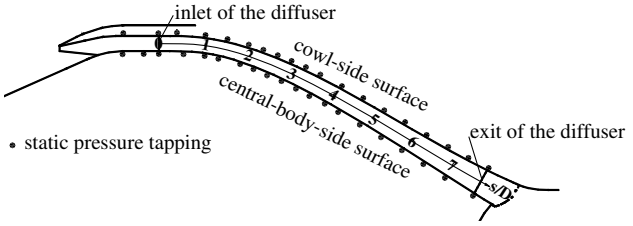

Fig. 5 Curvilinear coordinate attached on the central line of the diffuser.

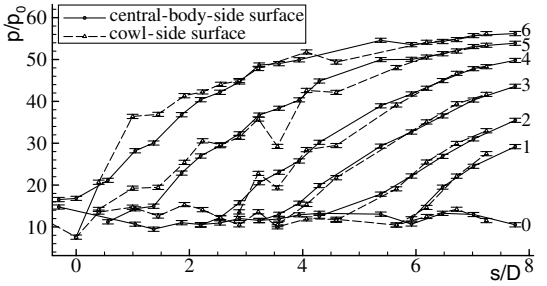

Fig. 6 Time-averaged surface pressure distributions of the diffuser at different backpressure conditions ($Ma_2 = 2.08$).

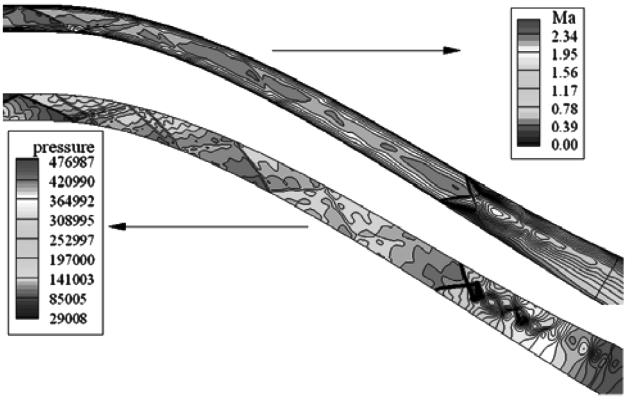

a) Shock train at the aft part of the diffuser

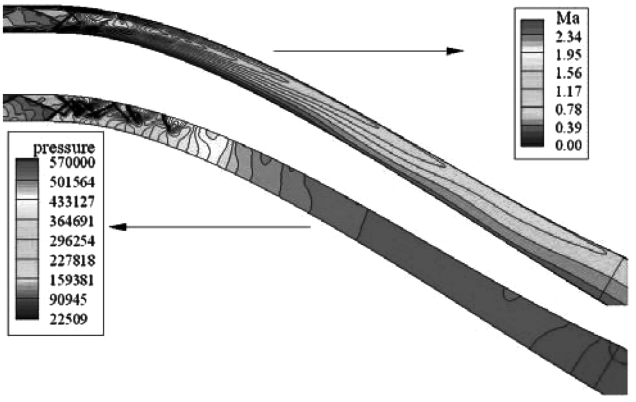

b) Shock train at the fore part of the diffuser

Fig. 7 Flow pattern of the shock train in a curved diffuser (CFD results, the inlet Mach number of the diffuser is 2.05).

2) After shifting to the fore of the diffuser, the shock train is no longer symmetric because of the remarkably increased local surface curvature, the asymmetrically distributed boundary layers, and the directional effects of the centrifugal force. There exist distinct differences between two fore legs of each bifurcated shock, such as

the originating surface position, the leg length, and the shock strength. In general, the bottom leg is longer and stronger than the top leg, which makes the boundary layer near the central-body-side surface even thicker and thereby results in a smooth surface pressure distribution. In contrast, because the supersonic core flow is obviously deflected to the cowl-side surface, the surface pressures of this side are readily affected by shock waves and expansion waves in the shock train and show large fluctuations along the flow direction. As to the flow region of $s/D > 6.0$, the dominant flow process is supersonic mixing or subsonic diffusing; therefore, the surface pressure distribution of the cowl side returns to a smooth trend.

A striking feature in Fig. 6 is the good similarity of the surface pressure distributions at different throttling ratios. The similarity implies that it is still possible to predict the static pressure rise in the shock train with a kind of modified Waltrup formula, even at this complicated situation of a curved variable-section diffuser with thick ingested boundary layer, strong incident oblique shock waves, and strong incident expansion waves. Based on the following facts and considerations, the experimental data are rearranged in a similar way, which is documented in [5].

1) Though there exist reflections of oblique shock waves and expansion waves in the duct, experimental data show that the Mach number difference between the inlet section (2.05) and the exit section (2.12) of the diffuser is small when TR = 0.0%. Therefore, the Mach number just upstream of the shock train at different TRs can be regarded as a constant, and a value of 2.08 is selected here.

2) The surface pressure variations along two sides are small when TR = 0.0%. So the average surface pressure can be employed as the initial pressure of the shock train (p_2), and a value of 11.3 times of the freestream pressure is used.

3) Computational fluid dynamics (CFD) results are used to obtain density and viscosity distributions that are needed in the calculation of Re_θ. Because the flow process involves boundary-layer transition, shock/boundary-layer interactions, and expansion wave/boundary-layer interactions, it is not easy to determine the boundary-layer-momentum-thickness distribution along the flow direction. Turbulent-plate boundary-layer developing law is adopted in this paper for a rough estimate of θ. The boundary-layer momentum thickness is selected as 0.8 mm at the inlet section of the diffuser ($s/D = 0$) and is assumed to develop at a four-fifths power law along the flow direction.

4) C_{mb} is introduced to correct the deviations of surface pressure distributions, which are caused by the complicated inlet conditions and the complicated geometric conditions from the Waltrup and Billing formula. That is to say, the original formula [5]

$$(M_2^2 - 1)(x/H)Re_\theta^{0.2}(H/\theta)^{0.5} = 50(p/p_2 - 1) + 170(p/p_2 - 1)^2$$

can be rewritten as

$$(M_2^2 - 1)\frac{s/D}{C_{mb}}Re_\theta^{0.2}(D/\theta)^{0.5} = 50(p/p_2 - 1) + 170(p/p_2 - 1)^2$$

where M_2 and p_2 are the average Mach number and the surface pressure just upstream of the shock train, respectively, and p is the local surface pressure. As can be seen, the introduction of C_{mb} is just to scale the relationship of pressure and s/D in a linear way. C_{mb} should be related to the surface curvature of the duct and is chosen as 1.32 in this paper.

The comparison of the rearranged experimental data and the pressure distributions predicted by the modified Waltrup formula is shown in Fig. 8. The data calculated by the original Waltrup formula are also plotted to provide a reference curve. As can be seen, dots at different backpressures cluster and agree well with the curve predicted by the modified formula with $C_{mb} = 1.32$. In other words, the shock-train length is increased by 32% due to the curved duct, the incident shock waves, and the incident expansion waves at the inlet of the diffuser. After a close view of the region with abscissa values below 300, one can notice that there are still small differences between the modified Waltrup curve and the data, indicating the need for further modifications of the formula.

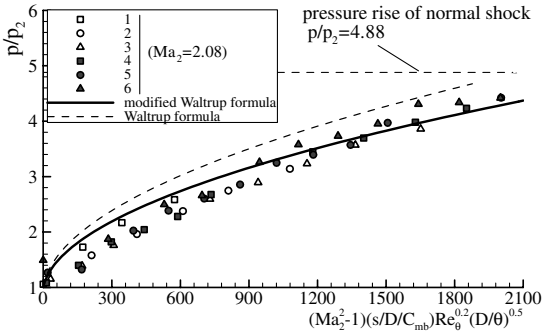

a) Central-body-side

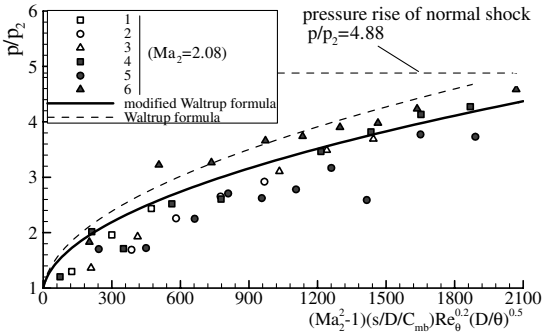

b) Cowl-side

Fig. 8 Comparison of the rearranged experimental data and the pressure distributions predicted by the modified Waltrup formula ($Ma_2 = 2.08$).

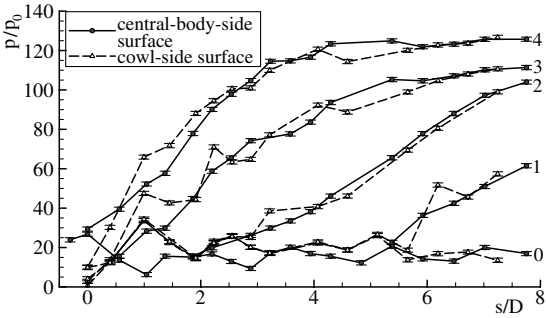

Fig. 9 Time-averaged surface pressure distributions of the diffuser at different backpressure conditions ($Ma_2 = 2.59$).

Time-averaged surface pressure distributions at freestream Mach numbers of 5.0 and 6.0 are shown in Figs. 9 and 10. The corresponding average inlet Mach numbers of the diffuser are 2.59 and 3.06. At the condition of free backpressure (curve 0), the streamwise fluctuations of the surface pressures become distinct with interlaced wave crests and troughs on either side, which indicates that the reflections of the incident shock waves, the incident expansion waves, and the waves induced by the curved surface bring significant influences on the surface pressure distributions. What's more, the similarities of the surface pressure distributions at different backpressure ratios disappear as a result of the strong interference of the incident shock waves and expansion waves. Therefore, the present formula cannot do a good job in predicting the surface pressure distributions (Fig. 11).

Figures 9 and 10 also demonstrate an important fact: the shock train is no longer symmetric wherever it stands when the curved diffuser operates at higher inlet Mach numbers. From the distinct fluctuations of surface pressures on the cowl side, it can be learned that the supersonic core flow region of the shock train is deflected to the cowl side. Fortunately, the start points of the shock train on both sides are very close and move upstream with the increase of TR

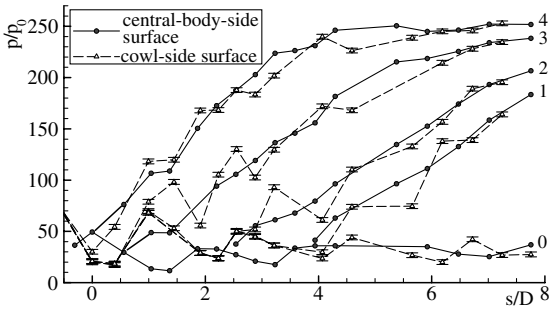

Fig. 10 Time-averaged surface pressure distributions of the diffuser at different backpressure conditions ($Ma_2 = 3.06$).

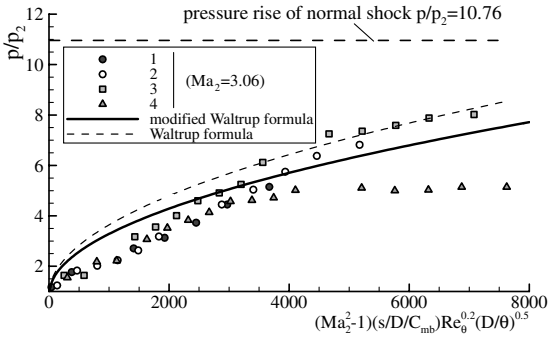

Fig. 11 Comparison of the rearranged experimental data and the pressure distribution predicted by modified Waltrup formula ($Ma_2 = 3.06$, central-body side).

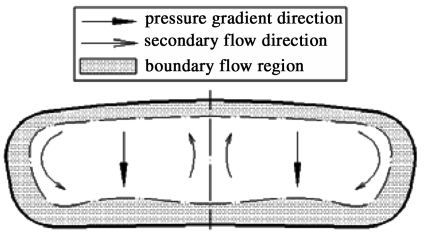

Fig. 12 Formation of swirl flow at the fore part of the diffuser.

almost synchronously, which can improve the backpressure limit of the diffuser.

From Figs. 6, 9, and 10, it can be noted that at the fore part of the diffuser ($s/D \leq 2.5$), the static pressure of the cowl side is almost always higher than that of the central-body side. This centrifugal pressure gradient with unchanged pointing direction results from the turning of the main flow. The gradient directs the low-momentum boundary flow toward the central-body side (Fig. 12) and generates two counter-rotating vortices that, in reverse, accumulate more and more boundary flow near the central-body side.

Time-Averaged Parameters at the Exit of the Diffuser

Based on the time-averaged data and a mass-weighted method [27], the total pressure recovery (Pt_e/Pt_2) and the Mach number at the exit of the diffuser are calculated and plotted against the backpressure ratios in Fig. 13. With the increase of the backpressure, the Mach number at the exit of the diffuser decreases monotonously. The obtained minimum exit Mach numbers at different inlet Mach numbers are all about 0.5. As to the total pressure recovery, the curves first show a remarkable drop and then a flat trend. The reasons are given as follows. When the backpressure is low, the shock train covers the exit section and any augment of the backpressure will make the shock train move forward, resulting in a stronger supersonic pressure-gain process upstream of the measurement plane. Therefore, both the total pressure recovery and the Mach

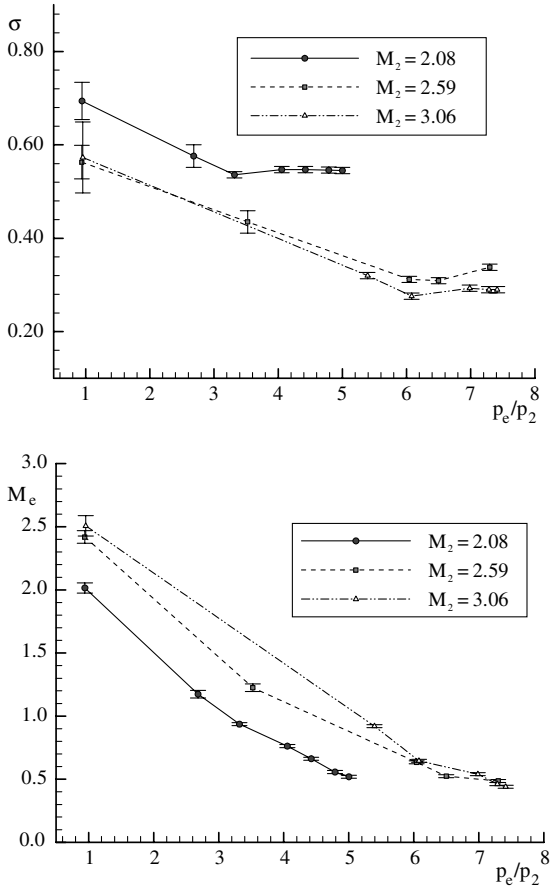

Fig. 13 Total pressure recovery coefficient and Mach number at the exit of the diffuser versus backpressure ratios.

number at the exit section decrease distinctly. When the backpressure exceeds a critical value, the shock train is entirely upstream of the exit section. The rise of the backpressure apparently affects the position of the shock train and the subsonic diffusion, but has little impact on the strength of the shock train, which, to a great extent, determines the total pressure loss. Thus, the total pressure recovery at the exit section is fairly stable.

The effects of inlet Mach numbers on the exit parameters can also be observed in Fig. 13. When the inlet Mach number increases from 2.08 to 2.59, the exit total pressure recovery descends and the backpressure limit evidently ascends, but a further increase of the inlet Mach number to 3.06 brings no perceptible change to the backpressure limit of the diffuser. In other words, the static pressure recovery performance of the shock train in the curved duct deteriorates remarkably when the inlet Mach number exceeds a critical value, which is not the case for straight ducts. So it can be inferred that the inlet Mach number of the curved diffuser should not exceed a value of around 2.59, to improve the overall backpressure performance of hypersonic inlets. In the design process of hypersonic inlets, this constraint can be met by adjusting the compression ratios obtained by the forebody and the contracting entrance.

Figure 14 exhibits the normalized pitot pressure distributions at the central line of the diffuser exit. The backpressure conditions correspond to curves 0 and 4 in Fig. 6. The pitot pressure profile at TR = 0.0% is slightly asymmetric, due to the ingested thick boundary layer near the central-body side. At large throttling ratios when the shock train originates from the fore of the diffuser, the deflected core flow and the unfavorable secondary flow lead to a noticeable asymmetric profile.

Distributions of Instantaneous Surface Pressure

To study the aerodynamic instability of the shock train in the curved duct, instantaneous surface pressure distributions are

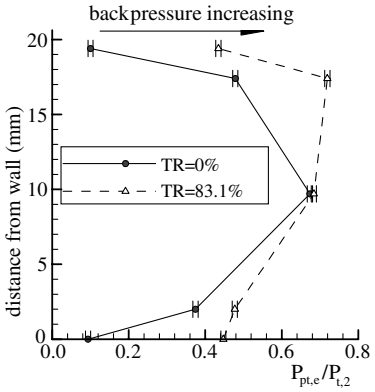

Fig. 14 Normalized pitot pressure at the central line of the diffuser exit versus distance from central-body-side surface ($Ma_2 = 2.08$).

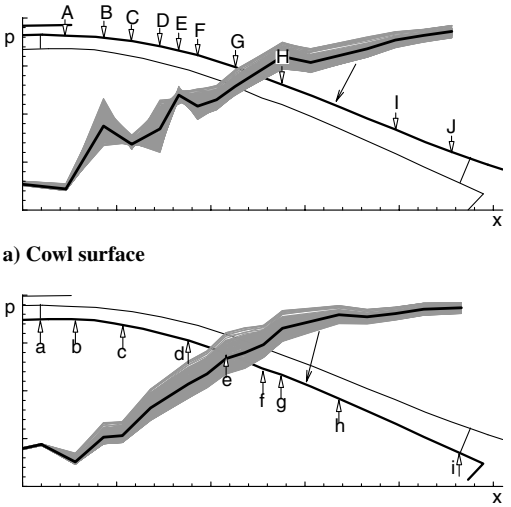

Fig. 15 Distributions of the instantaneous static pressure on both surfaces of the diffuser ($Ma_2 = 2.59$).

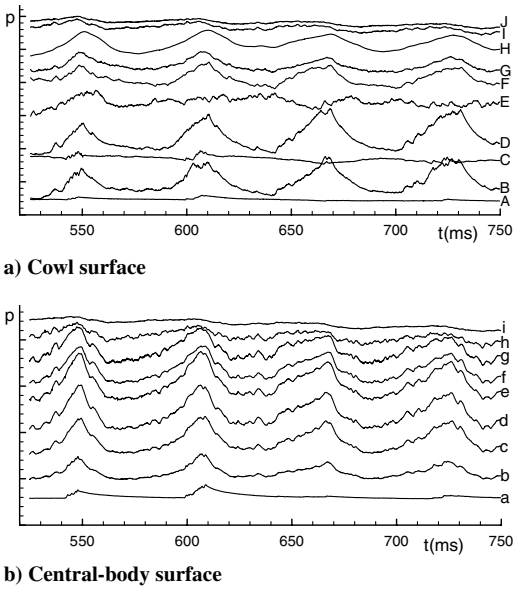

Fig. 16 Static pressure–time histories of typical survey points on both surfaces of the diffuser ($Ma_2 = 2.59$).

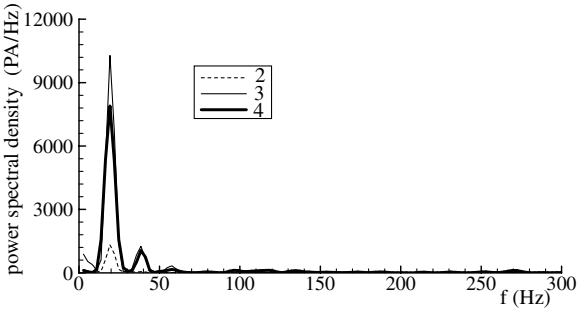

Fig. 17 Spectral density distributions of the instantaneous static pressures at different backpressure ratios (point D, $Ma_2 = 2.59$).

obtained with an integration period of 2 ms. The results in a period of 225 ms are plotted in Fig. 15. The diffuser operating conditions correspond to those of curve 3 in Fig. 9. The time-averaged results are also shown in Fig. 9 and are denoted by thick lines. Figure 15 shows that the instantaneous surface pressure distributions on both sides fluctuate around the time-averaged profiles all the time. In general, the amplitude of the surface pressure fluctuations is large in the middle of the shock train and small near two ends of the diffuser, except for two points (C and E) on the cowl side. The maximum amplitude of the fluctuating surface pressure on the central-body side is as high as 21.6% of the ideal pressure rise of the shock train. Furthermore, it can be inferred from the instantaneous pressure distributions that the strength and the length of the shock train change from moment to moment.

Figure 16 shows the pressure–time histories of several measurement points on both sides of the diffuser (refer to Fig. 15). Some curves were shifted vertically for tidiness. The striking features in Fig. 16 are the periodicity and the similarity of the pressure–time histories at different survey points. What's more, signals at different measurement points change almost synchronously, without any perceptible lag phase or leading phase. From Figs. 15 and 16, it can be concluded that the shock train oscillates along the flow direction at a specific base frequency. During these oscillations, the shock train is stretched and compressed from moment to moment. After a closer inspection of the top chart of Fig. 16, one can notice that two peculiar points marked by C and E, though in the shock train, demonstrate relative small fluctuations. A plausible explanation of this abnormality can be given as follows. Point C and point E are located just between two consecutive shocks and are not swept by either shock during the oscillations. So the surface pressures are not disturbed, apparently due to the thin boundary layer near the cowl side.

In Fig. 17, the power spectrum density distributions of the instantaneous pressure of point D at different backpressure ratios are plotted versus frequency. The backpressure conditions correspond to those of curves 2–4 in Fig. 9. Though the amplitudes are obviously different at different throttling ratios, the fluctuating energy distributions are similar, with a prominent peak at about 19 Hz.

Distributions of Root-Mean-Square Values of the Fluctuating Surface Pressures

In Fig. 18, the root-mean-square values of the fluctuating surface pressures are normalized by the inlet total pressure of the diffuser and plotted against the normalized streamwise position at different backpressure ratios. The charts are arranged in a backpressure ascending style. With the augment of the backpressure, the initial rise point of the p_{rms} distribution goes upstream gradually, which indicates the movement of the shock train. When the shock train is contained in the diffuser entirely, peaks of p_{rms} occur at the fore part of the shock train. Downstream of the shock train, p_{rms} tends to a nearly constant value, which is higher than that of the inlet flow. In the cases shown in Fig. 18, the maximum p_{rms} in the shock train is as high as 2.2% of the inlet total pressure of the diffuser, but the largest p_{rms} at the exit is below 0.5% of the inlet total pressure. This specific p_{rms} distribution decreases the possible threat of the sock train to the stable operation of the engine to some extent.

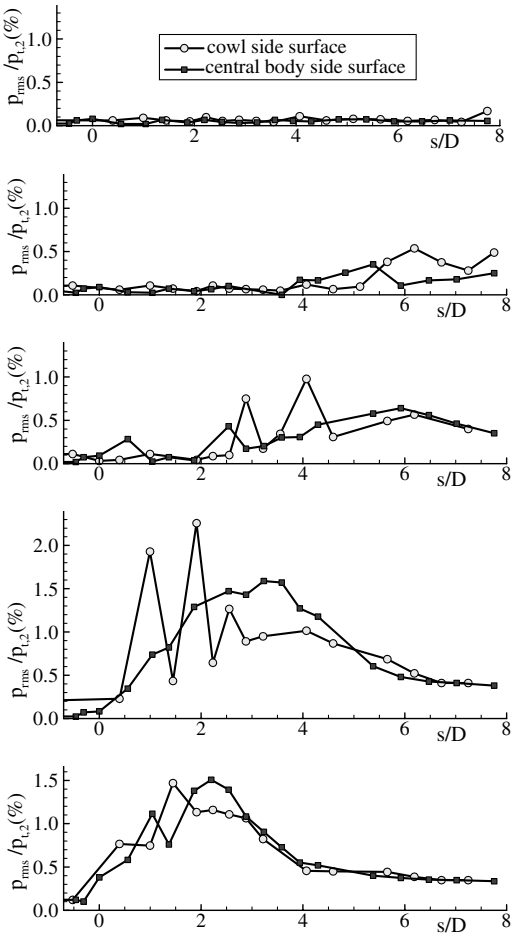

Fig. 18 Distributions of p_{rms} at different backpressure ratios ($Ma_2 = 2.59$).

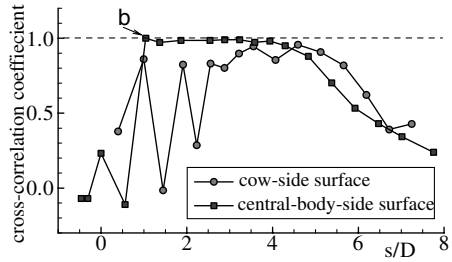

Fig. 19 Cross-correlation coefficients of the fluctuating surface pressures ($Ma_2 = 2.59$).

Another fact shown in Fig. 18 is that due to the deflected supersonic core flow and the local thin boundary layer near the cowl side, the p_{rms} distributions at the fore part of the cowl side fluctuate greatly and the maximum value of p_{rms} is higher than that of the central-body side.

Relationship Between Static Pressure Oscillations at Different Survey Points

The cross-correlation coefficients of fluctuating pressures are calculated with point B at different survey points on both surfaces and shown in Fig. 19. The flow conditions are the same as those of curve 3 in Fig. 9. Point B is just located at the leading edge of the shock train. It is thus found that the static pressure oscillations at point B are closely related to those of points in the shock train, with most values of cross-correlation coefficients above 0.8. The cross-correlation coefficients decrease gradually in the region of $s/D > 5.0$, in which the dominating flow processes are supersonic mixing and subsonic diffusing. The cross-correlation coefficient is only about 0.2 at the exit of the diffuser, suggesting that the pressure fluctuations at the exit section are nearly unrelated to those of point D and also to the motion of the shock train. So according to these results, the oscillations of the shock train are not likely induced by the pressure fluctuations far downstream of the shock train.

Conclusions

Wind-tunnel tests are performed to establish a preliminary knowledge of the behavior of the shock train in curved ducts. During tests, the diffuser is installed in a hypersonic inlet for the ramjet module of a dual-combustor ramjet. The inlet is tested at freestream Mach numbers of 4, 5, and 6, and the corresponding Mach numbers at the inlet section of the diffuser are 2.05, 2.59, and 3.06, respectively.

Compared with the situation in straight ducts, the shock train in the curved diffuser is obviously lengthened. When the inlet Mach number is 2.05, the shock-train length is increased by 32%, due to the curved duct, the incident shock waves, and the incident expansion waves at the inlet section of the diffuser. The surface pressure distribution of the shock train in the curved duct can be regarded as a linear stretching result of the pressure distribution in straight ducts. Therefore, it can be well predicted by the modified Waltrup formula after the introduction of a length scale factor. But at higher inlet Mach numbers of 2.59 and 3.06, the similarities of the surface pressure distributions in the shock train vanish, due to the strong interference of the incident shock waves, the incident expansion waves at the inlet section, and the waves caused by the curved surfaces. The instantaneous surface pressures in the shock train obviously fluctuate, due to the oscillatory motions of the shock train. At an inlet Mach number of 2.59, the spectral density distribution of the oscillations peaks at 19 Hz.

However, the geometry used in this paper is not a fundamental one and it is studied with the strong interference of incident shock waves and incident expansion waves at the inlet section. This impedes the flowfield visualization and adds difficulties in data analysis. Further work is planned to conduct experiments on a series of two-dimensional diffusers, including the variations of the surface curvature and the area divergent ratio.

Acknowledgments

This work is supported by the National Nature Science Foundation of the People's Republic of China through grant 50606017, the National Science Foundation for Postdoctoral Research of the People's Republic of China through grant 0601042B, and the Jiangsu Postdoctoral Sustentation Fund of the People's Republic of China through grant 20060400935.

References

[1] Matsuo, K., Miyazato, Y., and Kim, H. D., "Shock Train and Pseudo-Shock Phenomena in Internal Gas Flows," *Progress in Aerospace Sciences*, Vol. 35, No. 1, 1999, pp. 33–100. doi:10.1016/S0376-0421(98)00011-6

[2] Chyu, W. J., Kawamura, T., and Bencze, D. P., "Navier–Stokes Solutions for Mixed Compression Axisymmetric Inlet Flow with Terminal Shock," *Journal of Propulsion and Power*, Vol. 5, No. 1, 1989, pp. 4–5.

[3] Hamed, A., and Shang, J. S., "Survey of Validation Data Base for Shock Wave Boundary-Layer Interactions in Supersonic Inlets," *Journal of Propulsion and Power*, Vol. 7, No. 4, 1991, pp. 617–25.

[4] Sajben, M., Donovan, J. F., and Morris, M. J., "Experimental Investigation of Terminal Shock Sensors for Mixed-Compression Inlets," *Journal of Propulsion and Power*, Vol. 8, No. 1, 1992, pp. 168–74.

[5] Waltrup, P. J., and Billig, F. S., "Prediction of Precombustion Wall Pressure Distributions in Scramjet Engines," *Journal of Spacecraft and Rockets*, Vol. 0, No. 9, 1973, pp. 620–2.

[6] Curran, E. T., Heiser, W. H., and Pratt, D. T., "Fluid Phenomena in Scramjet Combustion Systems," *Annual Review of Fluid Mechanics*, Vol. 28, 1996, pp. 323–360. doi:10.1146/annurev.fl.28.010196.001543

[7] Matsuo, K., Sasaguchi, K., Mochizuki, H., and Takechi, N., "Investigation of the Starting Process of a Supersonic Wind Tunnel," *Bulletin of JSME*, Vol. 23, No. 186, 1980, pp. 1975–81.
[8] Carroll, B. F., and Dutton, J. C., "Characteristics of Multiple Shock Wave/Turbulent Boundary-Layer Interactions in Rectangular Ducts," *Journal of Propulsion and Power*, Vol. 6, No. 2, 1990, pp. 186–93.
[9] Stockbridge, R. D., "Experimental Investigation of Shock Wave/Boundary-Layer Interactions in an Annular Duct," *Journal of Propulsion and Power*, Vol. 5, No. 3, 1989, pp. 346–52.
[10] Gustafson, M. D., and Gruber, M. R., "Isolator Pressure Rise Correlations Compared with New Experimental Data," ISABE Paper 9927135, 1999.
[11] Lin, P., "Geometric Effects on Precombustion Shock Train in Constant Area Isolators," AIAA Paper 93-21838, 1993.
[12] Carroll, B. F., and Dutton, J. C., "Computations and Experiments for a Multiple Normal Shock/Boundary Layer Interaction," *Journal of Propulsion and Power*, Vol. 9, No. 3, 1993, pp. 405–411.
[13] Cox-Stouffer, S. K., "The Effect of Aspect Ratio on Isolator Performance," AIAA Paper 2001-0519, 2001.
[14] Katherine, M. G., "A Comparison Study of Rectangular and Chamfered Isolator Cross-Sectional Shape with Varied Divergence," AIAA Paper 2004-129, 2004.
[15] Fan, X. Q., Li, H., and Ding, M., "3-D Numerical Simulation on Inner Flow Field in Rectangular Cross Section Isolator," *Journal of Propulsion Technology*, Vol. 23, No. 2, 2002, pp. 129–131 (in Chinese).
[16] Li, H., Fan, X. Q., and Ding, M., "Numerical Simulation of the Shock Train Structure in the Supersonic Diffuser," *Journal of Propulsion Technology*, Vol. 24, No. 1, 2002, pp. 18–21 (in Chinese).
[17] Wang, C. P., Zhang, K. Y., Jin, Z. G., and Li, N., "Experimental Investigation on Internal Flow in Rectangular Isolator Under Non-Uniform Supersonic Flow," *Journal of Propulsion Technology*, Vol. 25, No. 4, 2004, pp. 349–353 (in Chinese).
[18] Wang, C. P., Zhang, K. Y., and Cheng, K. M., "Pressure Distribution Measurements in Scramjet Isolator Under Asymmetric Supersonic Flow," AIAA Paper 2006-0818, 2006.
[19] Tan, H. J., and Guo, R. W., "Characteristics of Shock Train in Two Dimensional Bends with Constant Area," *Acta Aeronautica et Astronautica Sinica*, Vol. 27, No. 6, 2006, pp. 1039–1045.
[20] Gnos, A. V., Watson, E. C., Seebaugh, W. R., Sanator, R. J., and DeCarlo, J. P., "Investigation of Flow Fields Within Large-Scale Hypersonic Inlet Models," NASA TR TND-7150, Apr. 1973.
[21] Billing, F. S., Waltrup, P. J., and Stockbrige, R. D., "Integral-Rocket Dual-Combustion Ramjets: A New Propulsion Concept," *Journal of Spacecraft and Rockets*, Vol. 17, No. 5, 1980, pp. 416–424.
[22] DeBonis, J. R., and Trefny, C. J., "Supersonic Wind Tunnel Tests of a Half-Axisymmetric 12°-Spike Inlet to a Rocket-Based Combined-Cycle Propulsion System," NASA TM-2001-210567, Feb. 2001.
[23] Ohshima, T., and Enomoto, Y., "Experimental Approach to HYPR Mach 5 Ramjet Propulsion System," AIAA Paper 1998-3277, 1998.
[24] Kojima, T., Tanatsugut, N., Satoij, T., and Kanda, M., "Development Study on Axisymmetric Air Inlet for Atrex Engine," AIAA Paper 2001-1895, 2001.
[25] Matsuo, K., and Mochizuki, H., "Oscillatory Characteristics of a Pseudo-Shock Wave in a Rectangular Straight Duct," *JSME International Journal, Series B (Fluids and Thermal Engineering)*, Vol. 36, No. 2, 1993, pp. 222–229.
[26] Tan, H. J., and Guo, R. W., "Experimental Study of the Unstable-Unstarted Condition of a Hypersonic Inlet at Mach 6," *Journal of Propulsion and Power*, Vol. 23, No. 4, 2007, pp. 783–788. doi:10.2514/1.28039
[27] Seddon, J., and Goldsimith, E. L., *Intake Aerodynamics*, AIAA Education Series, AIAA, Washington, DC, 1985, pp. 375–376.

R. Bowersox
Associate Editor